Advance Publication

IEEJ Journal of Industry Applications
J-STAGE Advance published date : Jan. 28, 2022
DOI : 10.1541/ieejjia.21005686

Paper

Derivation of Dynamic Model of Two-Input-Two-Output Torque Difference Amplification Motor Drive System and Independent Left-and-Right Wheel Control with Decoupling Compensator

Hiroyuki Fuse*a) Student Member, Hiroshi Fujimoto* Senior Member
Kaoru Sawase** Non-member, Naoki Takahashi** Non-member
Ryota Takahashi** Non-member, Yutaro Okamura** Non-member
Ryosuke Koga** Non-member

(Manuscript received May 10, 2021, revised September 22, 2021)

A torque vectoring differential (TVD) enhances the cornering performance by generating a torque difference between the left and right wheels. For electrified vehicles, a TVD with a two-motor-torque difference amplification mechanism (TDA-TVD) is proposed, and it generates a greater torque difference than an Individual-wheel-drive (IWD) system under the same power output from the traction motors. However, owing to the complex gear reduction system including planetary gears and driveshafts, TDA-TVD has problems with the vibration of both the driveshaft torque and the yaw rate while cornering. To deal with these problems, a detailed dynamic model of TDA-TVD is first derived in this study. Secondly, a decoupling compensator is designed to achieve independent drive for the left and right wheels so that any motor drive algorithm designed for IWD systems can be applied. Thirdly, a vibration suppression controller is designed. Then, simulations and experimental evaluations using a real vehicle with the TDA-TVD are performed. The experimental results show the effectiveness of the vibration suppression of driveshafts and yaw rate.

Keywords: Electric Vehicle, Motor Drive System, Two-Input-Two-Output System, Vibration Suppression, Decoupling Compensation, Torque Vectoring Differential

Nomenclature

M	Vehicle mass
r	Effective wheel radius
J_ω	Wheel inertia
J_m	Motor inertia
J_{all}	Nominal wheel inertia
G	Primary reduction gear ratio
b_1, b_2	Equivalent secondary reduction gear ratio
K_s	Stiffness of driveshaft
D_s	Damping factor of driveshaft
T_{RM}, T_{LM}	Input motor torque (R: right side, L: left side)
T_{RDm}, T_{LDm}	Input motor torque after primary gear reduction
T_{Rm}, T_{Lm}	Transmitted motor torque to planetary gears
T_{RIm}, T_{LIm}	Motor inertia torque
T_{Rin}, T_{Lin}	Input motor torque converted to driveshaft side
T_{Rds}, T_{Lds}	Driveshaft torque after secondary gear reduction
ω_{RM}, ω_{LM}	Motor side angular speed before primary gear reduction
ω_{Rm}, ω_{Lm}	Motor side angular speed after primary gear reduction
ω_{Rds}, ω_{Lds}	Driveshaft side angular speed after secondary gear reduction
λ	slip ratio

a) Correspondence to: fuse.hiroyuki17@ae.k.u-tokyo.ac.jp
* Department of Advanced Energy, The University of Tokyo. 7H1, Transdisciplinary Sciences Bldg.,5-1-5, Kashiwanoha, Kashiwa, Chiba, Japan, 277–8561
** MITSUBISHI MOTORS CORPORATION 1, Nakashinkiri, Hashimecho, Okazaki, Aichi, Japan, 444–8501

1. Introduction

A torque vectoring differential (TVD) is a device that controls direct yaw moment by generating a torque difference between the left and right wheels. TVD has the advantage of improving the cornering performance by actively controlling the yaw moment [1] [2] [3].

For that reason, some electric vehicles adopt individual-wheel-drive (IWD) systems (either with on-board or in wheel motor, as seen in Fig. 1(a)) and a lot of torque vectoring or distribution algorithms have been studied [4] [5] [6]. However, the maximum available torque difference and direct yaw moment decrease when the vehicle is at high speed, and the same problem occurs when the vehicle is cornering near the critical region, due to the decreased traction of the inner wheels caused by the load transfer.

A TVD with a two-motor-torque difference amplification mechanism (TDA-TVD) has been proposed in order to increase the maximum available torque difference [7] [8]. TDA-TVD drives two wheels with two motors, but unlike conventional IWD vehicles, there is a mechanical coupling between the left and right wheels as seen in Fig. 1(b). Therefore, TDA-TVD is categorized as a two-input-two-output drive system. Thanks to the mechanical coupling, TDA-TVD can generates greater torque differences between the left and right wheels compared to the IWD system with the same electric traction motor (i.e., torque difference amplitude fac-

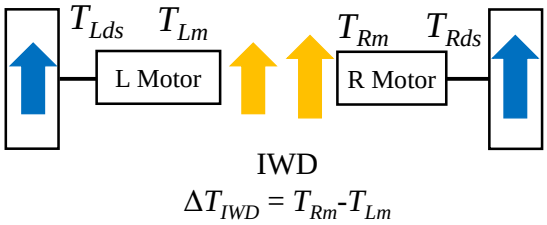

(a) Individually driven wheel (IWD) system.

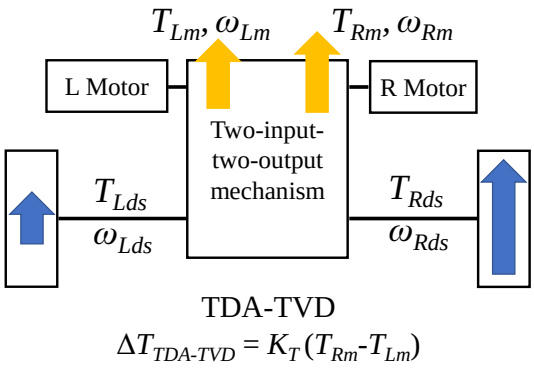

(b) Two-motor-torque difference amplification TVD system (TDA-TVD).

Figure 1: Torque vectoring differentials. TDA-TVD can generate greater torque difference ΔT than IWD system (Torque difference amplification factor $K_T > 1$).

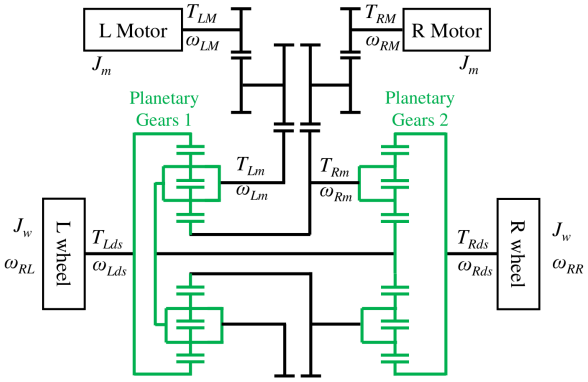

Figure 2: Schematic diagram of TDA-TVD [8].

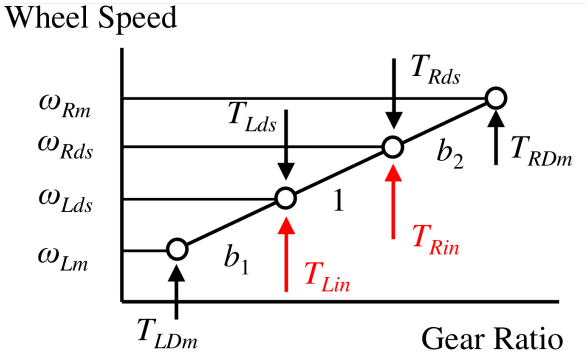

Figure 3: Velocity diagram of TDA-TVD.

tor $K_T > 1$ in Fig. 1) and overall cornering maneuverability. However, while TDA-TVD has the same advantages as the TVD, it has relatively complex mechanical components, including planetary gears, reduction gears, and driveshafts. This leads to undesirable vibrations of the driveshaft torque on the wheels and yaw rate vibration while cornering with its torque vectoring system in function. The previous study [7] [8] did not derive the dynamic model of TDA-TVD that describes its anticipated vibrations of the driveshaft torque and yaw motion.These problems limit the performance of TDA-TVD and must be solved in order to achieve its full potential.

Vibration suppression in vehicles has been widely studied for a long time because they have a lot of vibrating components such as internal combustion engines, transmissions, driveshafts, and tires. In the case of EVs, even though their driveline tends to be simpler than internal combustion engine vehicles (ICVs), the relatively fast torque response of electric motors can create uncomfortable shaking vibration originating from the driveshafts when referring to on-board EVs. In order to deal with these problems, various anti-jerk controllers have been studied and proposed [9] [10] [11]. Each study basically constructs a certain dynamic model of the driveline of the target EVs and implements either or both a feedback and a feedforward controller. A majority of these studies consider EVs with a single-input-single-output drive system (e.g., a single on-board motor drives the two front or rear wheels, or single on-board or in-wheel motor drives the left or right wheel individually). Therefore, these studies cannot be directly applied to TDA-TVD due to the difference in the mechanical structure .

First, this study constructs a detailed dynamic model of TDA-TVD to describe the mechanical coupling of its drive system between the left and right wheels. Next, this study designs a decoupling compensator that enables us to control the left and right wheels independently, based on the obtained dynamic model of TDA-TVD. With the decoupling compensator, we can apply conventional vibration suppression controls originally designed for IWD systems. This way, we can treat TDA-TVD as an IWD system and the overall vehicle dynamics control system will be significantly simpler.

As a demonstration of the validity of the obtained dynamic model of TDA-TVD and decoupling compensator, a simple feedforward vibration suppression controller based on the inverse model of the decoupled drive system is designed, simulated, and experimentally tested.

The rest of this paper is as follows. First, a dynamic model of TDA-TVD is obtained. Second, the decoupling compensator and feedforward vibration suppression controller are designed. Third, simulations and experimental evaluations using a real vehicle that is equipped with TDA-TVD are demonstrated. Their results are analyzed and show the validity of the derived dynamic model and effectiveness of the proposed decoupling compensator and implemented vibration suppression control.

2. Derivation of the dynamic model of TDA-TVD

Several types of TDA-TVD have been proposed by Sawase [7] [8]. As an example of those, a schematic diagram of TDA-TVD is shown in Fig. 2. Regardless of the different types of TDA-TVD, the following equations can be derived comprehensively. The motor torques T_{RM} and T_{LM} are amplified by the primary gear ratio G through the primary reduction gears and become T_{RDm} and T_{LDm}, respectively. After

passing through the following planetary gears, the driveshaft torques T_{Rds} and T_{Lds} are transmitted to the wheels. The relation of the rotation speed and torque is visually represented by a velocity diagram as shown in Fig. 3 [8]. In the figure, b_1 and b_2 are the equivalent secondary reduction gear ratios determined by each gear of the planetary gears. b_1 and b_2 are designed to be almost equal. From Fig. 3, we have the following equations

$$T_{Rin} = (b_2 + 1)T_{RDm} - b_1 T_{LDm} \cdots (1)$$
$$T_{Lin} = (b_1 + 1)T_{LDm} - b_2 T_{RDm} \cdots (2)$$

where T_{Rin} and T_{Lin} are the input motor torque imaginarily converted to the driveshaft side. T_{Rin} and T_{Lin} are convenient to deal with the mechanical coupling which will be explained later. T_{Rm} and T_{Lm} in Fig. 2 are the transmitted motor torques to the planetary gears after the gear reduction and represented by

$$T_{Rm} = T_{RDm} - T_{RIm} \cdots (3)$$
$$T_{Lm} = T_{LDm} - T_{LIm} \cdots (4)$$
$$T_{RIm} = G^2 J_m \dot{\omega}_{Rm} \cdots (5)$$
$$T_{LIm} = G^2 J_m \dot{\omega}_{Lm} \cdots (6)$$

where T_{RIm} and T_{LIm} are inertia torques of the motor, J_m is the inertia of the motor, and ω_{Rm} and ω_{Lm} are the motor side angular speeds after the primary gear reduction. ω_{Rm}, ω_{Lm} and the driveshaft side angular speeds ω_{Rds} and ω_{Lds} have the following relations

$$\omega_{Rm} = (b_2 + 1)\omega_{Rds} - b_2 \omega_{Lds} \cdots (7)$$
$$\omega_{Lm} = -b_1 \omega_{Lds} + (b_1 + 1)\omega_{Rds}. \cdots (8)$$

2.1 Derivation of the linearized model This section derives the linearized model of TDA-TVD. From the equations of TDA-TVD shown earlier, we can derive the following equations using matrices and vectors

$$J\dot{\omega}_{ds} = T_{in} - T_{ds} \cdots (9)$$

where

$$J = \begin{pmatrix} J_{11} & J_{12} \\ J_{21} & J_{22} \end{pmatrix} \cdots (10)$$
$$J_{11} = [(b_2 + 1)^2 + b_1^2]G^2 J_m \cdots (11)$$
$$J_{12} = J_{21} = -[b_1(b_1 + 1) + b_2(b_2 + 1)]G^2 J_m \cdots (12)$$
$$J_{22} = [(b_1 + 1)^2 + b_2^2]G^2 J_m \cdots (13)$$
$$\dot{\omega}_{ds} = \begin{pmatrix} \dot{\omega}_{Rds} \\ \dot{\omega}_{Lds} \end{pmatrix} \cdots (14)$$
$$T_{in} = \begin{pmatrix} T_{Rin} \\ T_{Lin} \end{pmatrix} = KT_m \cdots (15)$$
$$K = \begin{pmatrix} k_{11} & k_{12} \\ k_{21} & k_{22} \end{pmatrix} = \begin{pmatrix} b_2 + 1 & -b_1 \\ -b_2 & b_1 + 1 \end{pmatrix} \cdots (16)$$
$$T_m = \begin{pmatrix} T_{RDm} \\ T_{LDm} \end{pmatrix} \cdots (17)$$
$$T_{ds} = \begin{pmatrix} T_{Rds} \\ T_{Lds} \end{pmatrix} \cdots (18)$$

In this paper, we assume that all the elasticity and viscosity of TDA-TVD are equivalently represented by the driveshaft stiffness K_s and damping factor D_s. With this assumption, the driveshaft torque T_{jds} (subscript j is either l (left) or r (right)) and the driveshaft angular speed ω_{jds} have the following relations [11] [12]

$$T_{jds} = \left(\frac{K_s}{s} + D_s\right)(\omega_{jds} - \omega_{Rj}) \cdots (19)$$
$$\omega_{Rj} = \frac{T_{jds}}{J_{all}s} \cdots (20)$$
$$J_{all} = J_w + r^2 M(1 - \lambda_n)/2, \cdots (21)$$

where ω_{Rj} is the angular speed of the rear wheel, J_{all} is the nominal inertia of the wheel at the nominal slip ratio λ_n (0: when the wheel is not slipping, 1: when the wheel is slipping), r is the effective radius of the wheel, and M is the vehicle mass. Assuming that the wheel rotates at the nominal slip ratio λ_n, the nonlinear dynamics between the wheel and the road can be linearized. From (19) and (20), we get the following equation

$$\dot{\omega}_{ds} = \frac{J_{all}s^2 + D_s s + K_s}{J_{all}(D_s s + K_s)} T_{ds}. \cdots (22)$$

By substituting (22) to (9), we have

$$\left(E_2 + \frac{J_{all}s^2 + D_s s + K_s}{J_{all}(D_s s + K_s)} J\right) T_{ds} = T_{in} \cdots (23)$$

where E_2 is an identity matrix of size 2. Here, we define a matrix g given by

$$g = \begin{pmatrix} g_{11} & g_{12} \\ g_{21} & g_{22} \end{pmatrix} = \left(E_2 + \frac{J_{all}s^2 + D_s s + K_s}{J_{all}(D_s s + K_s)} J\right)^{-1} \cdots (24)$$

Now we have

$$T_{ds} = gT_{in} \cdots (25)$$
$$\begin{pmatrix} T_{Rds} \\ T_{Lds} \end{pmatrix} = \begin{pmatrix} g_{11} & g_{12} \\ g_{21} & g_{22} \end{pmatrix} \begin{pmatrix} T_{Rin} \\ T_{Lin} \end{pmatrix} \cdots (26)$$

From the above equation, we can derive the four transfer functions as follows

$$\frac{T_{Rds}}{T_{Rin}} = g_{11} = \frac{g_{11n}}{g_d} \cdots (27)$$
$$\frac{T_{Rds}}{T_{Lin}} = g_{12} = \frac{g_{12n}}{g_d} \cdots (28)$$
$$\frac{T_{Lds}}{T_{Rin}} = g_{21} = g_{12} \cdots (29)$$
$$\frac{T_{Lds}}{T_{Lin}} = g_{22} = \frac{g_{22n}}{g_d} \cdots (30)$$
$$g_{11n} = J_{all}\{J_{22}J_{all}s^3 + ((J_{22} + J_{all})D_s^2 + J_{22}J_{all}K_s)s^2 \cdots (31)$$
$$+ 2K_s D_s(J_{22} + J_{all})s + K_s^2(J_{22} + J_{all})\}$$
$$g_{12n} = g_{21n} = -J_{12}J_{all}(J_{all}D_s s^3 \cdots (32)$$
$$+ (J_{all}K_s + D^2)s^2 + 2K_s D_s s + K_s^2)$$
$$g_{22n} = J_{all}\{J_{11}J_{all}s^3 + ((J_{11} + J_{all})D_s^2 \cdots (33)$$
$$+ J_{11}J_{all}K_s)s^2 + 2K_s D_s(J_{11} + J_{all})s + K_s^2(J_{11} + J_{all})\}$$
$$g_d = |J|J_{all}^2 s^4 + J_{all}D_s(2|J| + (J_{11} + J_{22})J_{all})s^3 \cdots (34)$$
$$+ (|J|(2J_{all}K_s + D^2) + J_{all}(J_{11} + J_{22})(D_s^2 + J_{all}K_s)$$
$$+ J_{all}^2 D_s^2)s^2 + 2K_s D_s(|J| + (J_{11} + J_{22})J_{all} + J_{all}^2)s$$

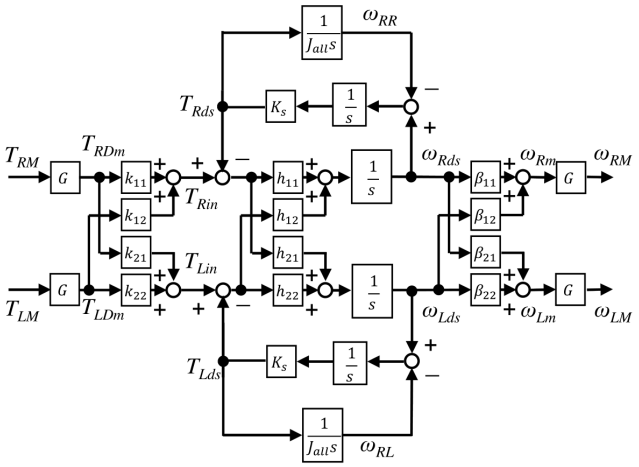

Figure 4: Block diagram of TDA-TVD.

$$+ K_s^2(|J| + (J_{11} + J_{22})J_{all} + J_{all}^2)$$
$$|J| = J_{11}J_{22} - J_{12}J_{21} = G^4 J_m^2(b_1 + b_2 + 1)^2. \cdots (35)$$

Now we have obtained the linear model of TDA-TVD. The block diagram of TDA-TVD is represented in Fig. 4. In the figure, the following relations are given to represent the parameters.

$$J^{-1} = \frac{1}{|J|}\begin{pmatrix} J_{22} & -J_{12} \\ -J_{21} & J_{11} \end{pmatrix} = \begin{pmatrix} h_{11} & h_{12} \\ h_{21} & h_{22} \end{pmatrix} \cdots\cdots\cdots (36)$$

$$\begin{pmatrix} \omega_{Rm} \\ \omega_{Lm} \end{pmatrix} = \begin{pmatrix} b_2 + 1 & -b_2 \\ -b_1 & b_1 + 1 \end{pmatrix}\begin{pmatrix} \omega_{Rds} \\ \omega_{Lds} \end{pmatrix} \cdots\cdots\cdots\cdots (37)$$
$$= \begin{pmatrix} \beta_{11} & \beta_{12} \\ \beta_{21} & \beta_{22} \end{pmatrix}\begin{pmatrix} \omega_{Rds} \\ \omega_{Lds} \end{pmatrix} = B\begin{pmatrix} \omega_{Rds} \\ \omega_{Lds} \end{pmatrix}$$

3. Design of the joint torque controller for TDA-TVD

This section derives and designs a joint torque controller (JTC) for TDA-TVD that suppresses the driveshaft torque vibration. The JTC is composed of a driveshaft-motor torque converter, a decoupling compensator, and a feedforward controller.

3.1 Design of the driveshaft-motor torque converter TDA-TVD has the two inputs T_{RM} and T_{LM} which we can freely control, and two outputs ω_{RM} and ω_{LM} as the obtainable values through the drive-side angular speed sensor which are used to drive the electric motors.

In order to control the converted motor-side torque inputs T_{Rin} and T_{Lin} and estimate the driveshaft angular speeds ω_{Rds} and ω_{Lds}, we can utilize the following relations from (15), (16), and (38)

$$\begin{pmatrix} \omega_{Rds-\mathrm{est}} \\ \omega_{Lds-\mathrm{est}} \end{pmatrix} = G^{-1}B^{-1}\begin{pmatrix} \omega_{RM} \\ \omega_{LM} \end{pmatrix} \cdots\cdots\cdots\cdots (38)$$

$$\begin{pmatrix} T_{RM} \\ T_{LM} \end{pmatrix} = G^{-1}K^{-1}\begin{pmatrix} T_{Rin-\mathrm{ref}} \\ T_{Lin-\mathrm{ref}} \end{pmatrix} \cdots\cdots\cdots\cdots (39)$$

The second equation is called "driveshaft-motor torque converter" (DMTC) and it is shown in the left side block diagram of the Fig. 5 (which is $G^{-1}K^{-1}$, colored light blue). The first equation is called "driveshaft angular speed estimator" (DSE) and it is shown as the red colored $G^{-1}B^{-1}$ in the Fig. 5.

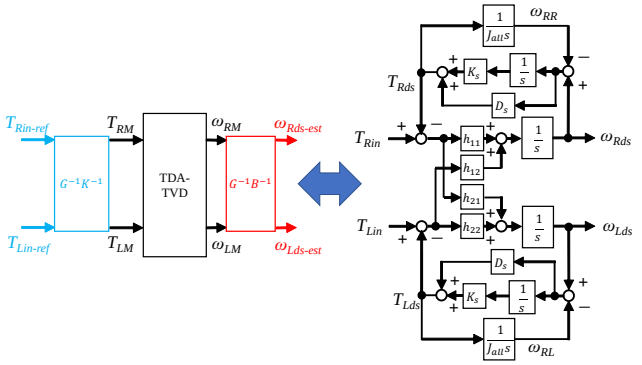

Figure 5: Driveshaft-motor torque converter (colored light blue) and driveshaft angular speed estimator (colored red) of TDA-TVD and simplified block diagram.

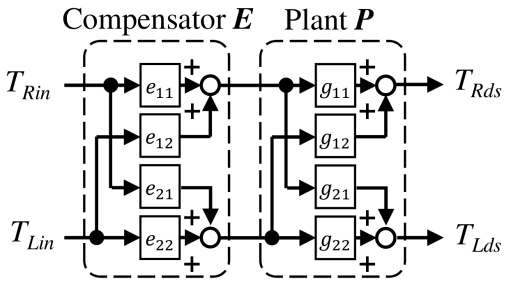

Figure 6: Decoupling compensator E is inserted before TDA-TVD (Plant P).

With this DMTC, the driveshaft torque can be controlled, but with slight errors due to the inertia torque of the motors and the coupling. Some sort of wheel speed control or anti-skid-wheel control can be implemented and achieved with the DMTC. However, as mentioned earlier, due to the elasticity and viscosity of TDA-TVD, an undesirable vibration is inevitable. The DMTC will be also called a base controller in the later simulations and experiments.

3.2 Design of the decoupling compensator In order to directly control the driveshaft torque itself, we need to construct a decoupling compensator so that the left and right wheels can be independently controlled. The decoupling compensator E is added before the direct torque controller, as shown in Fig. 6. In the figure, the plant P is the TDA-TVD with the DMTC shown in Fig. 5, but the outputs are the driveshaft torques. Thankfully, there is a traditional method called "diagonalization" of multi-input-multi-output systems [13] and each gain of the decoupling compensator E is given by

$$e_{11} = e_{22} = 1 \cdots\cdots\cdots\cdots (40)$$
$$e_{12} = -\frac{g_{12}}{g_{11}} = -\frac{g_{12n}}{g_{11n}} \cdots\cdots\cdots\cdots (41)$$
$$e_{21} = -\frac{g_{21}}{g_{22}} = -\frac{g_{12n}}{g_{22n}} \cdots\cdots\cdots\cdots (42)$$

Now, the transfer functions with the decoupling compensator E are obtained as follows

$$\frac{T_{Rds}}{T_{Rin}} = \frac{J_{all}(D_s s + K_s)}{J_{11}J_{all}s^2 + D_s(J_{11} + J_{all})s + K_s(J_{11} + J_{all})} \cdots (43)$$

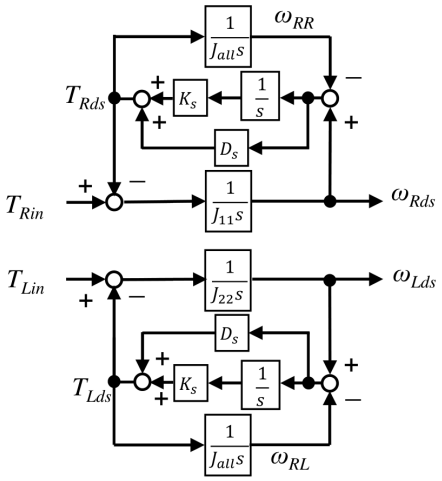

Figure 7: Equivalent block diagram of TDA-TVD with decoupling compensator E.

$$\frac{T_{Rds}}{T_{Lin}} = \frac{T_{Lds}}{T_{Rin}} = 0 \cdots\cdots (44)$$

$$\frac{T_{Lds}}{T_{Lin}} = \frac{J_{all}(D_s s + K_s)}{J_{22}J_{all}s^2 + D_s(J_{22}+J_{all})s + K_s(J_{22}+J_{all})} \cdots (45)$$

The equivalent block diagram of TDA-TVD with the decoupling compensator E is shown in Fig. 7. It clearly suggests that the left and right wheels can be controlled independently.

The transfer functions of the decoupled system have second order characteristic polynomials. The decoupled system has a pair of conjugate complex roots $-\alpha \pm j\beta$ ($j = \sqrt{-1}$) given by

$$\alpha = \frac{D_s(J_M + J_{all})}{2J_M J_{all}} \cdots\cdots (46)$$

$$\beta = \frac{1}{2}\sqrt{\frac{J_M + J_{all}}{J_M J_{all}}\left(4K_s - \frac{D_s(J_M + J_{all})}{J_M J_{all}}\right)} \cdots\cdots (47)$$

where J_M is either J_{11} or J_{22}. The step response of the decoupled system ($T_{jin}(t) = 1$) is given by

$$T_{jds}(t) = \frac{J_{all}}{J_M + J_{all}}\left(1 - e^{-\alpha t}\cos\beta t\right) + \frac{D_s}{2J_M\beta}e^{-\alpha t}\sin\beta t$$
$$\approx \frac{J_{all}}{J_M + J_{all}}\left(1 - e^{-\alpha t}\cos\beta t\right) \cdots\cdots (48)$$

The equation suggests that the final value will have a slight error due to the motor side inertia. With the typical parameters as shown in Tab. 1, we can assume $J_M \ll J_{all}$ and $4J_M K_s \gg D_s$ and we can derive $\frac{J_{all}}{J_M+J_{all}} \approx 1$ and $\frac{D_s}{2J_M\beta} \approx \frac{D_s}{2\sqrt{J_M K_s}} < \frac{1}{10}$. Therefore, the second term of the right side of this equation is negligible compared to the first term. The normalized overshoot of the step response of the decoupled system OS is obtained by substituting $t = \pi/\beta$ to (48) as follows

$$OS = e^{-\alpha\pi/\beta} \cdots\cdots (49)$$

As an example, a vehicle with typical parameters as shown in Tab. 1 has a driveshaft vibration frequency of $\beta/(2\pi) = 2.922$ Hz, and the normalized overshoot $OS = 0.749$ ($J_M = J_{11}$). This causes undesirable driveshaft and yaw rate vibrations that must be suppressed.

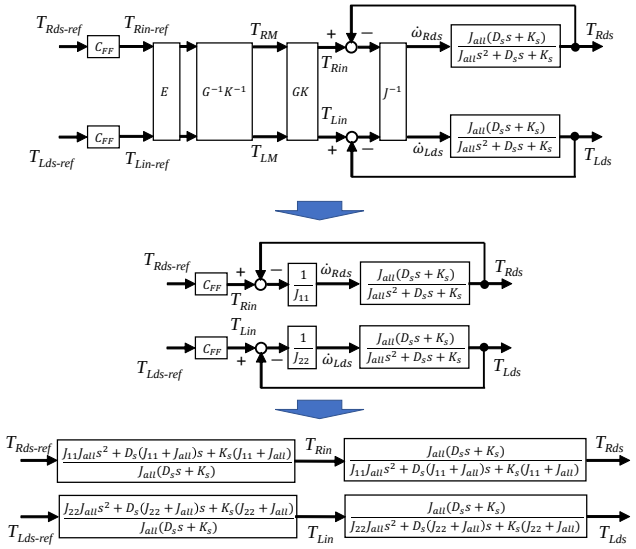

Figure 8: Block diagram of TDA-TVD with feedforward.

3.3 Design of the feedforward controller A feedforward controller is designed by the inverse of the transfer function of the decoupled system $\frac{T_{jin}}{T_{jds}}$ [12], which is given by

$$C_{FF} = \frac{J_M J_{all}s^2 + D_s(J_M + J_{all})s + K_s(J_M + J_{all})}{J_{all}(D_s s + K_s)} \cdots (50)$$

Since C_{FF} is not proper, a low pass filter (LPF) Q_{FF} is added. With this feedforward controller, the decoupling compensator and the DMTC, the transfer function $\frac{T_{jds}}{T_{jds-ref}}$ becomes a unity (i.e., 1) so that undesirable vibration could be suppressed, which is shown in Fig. 8.

A feedback controller can also be designed and implemented in the same way with [12]. However, in order to evaluate the derived dynamic model and the decoupling compensator of TDA-TVD, this study only implements the feedforward controller for the simulations and experiments.

4. Simulations of the joint torque controller for TDA-TVD

Simulations of the JTC for TDA-TVD is conducted using MATLAB and Simulink environment. The wheel model is approximated by a linear model as shown in Fig. 4.

4.1 Simulation conditions In order to evaluate the performance of the JTC, the base controller without the JTC, the JTC with the feedforward and the decoupling compensator are tested. For comparison, the modified JTC which only considers inertia (JTC–s0) and given by the following equations

$$e_{12\text{–}s0} = \frac{J_{12}}{J_{22} + J_{all}} \cdots\cdots (51)$$

$$e_{21\text{–}s0} = \frac{J_{12}}{J_{11} + J_{all}} \cdots\cdots (52)$$

$$C_{FF\text{–}s0} = \frac{J_M + J_{all}}{J_{all}}, \cdots\cdots (53)$$

is also tested. These equations can be simply obtained by substituting $s = 0$ to the equations of the decoupling compensator and the feedforward controller.

Table 1: Simulated vehicle parameters.

Vehicle mass M	1500 kg
Effective wheel radius r	0.35 m
Wheel inertia J_ω	1.5 kg·m^2
Motor inertia J_m	0.02 kg·m^2
Primary reduction gear ratio G	12
Equivalent secondary reduction gear ratio b_1, b_2	0.7, 0.71
Stiffness of driveshaft K_s	3000 N/rad
Damping factor of driveshaft D_s	30 N/(rad/s)
Nominal slip ratio λ_n	0
Nominal wheel inertia J_{all}	93.38 kg·m^2
Inertia matrix J_{11}, J_{12}, J_{22}	9.83, -6.92, 9.77 kg·m^2
Step response parameters α, β, OS $(J_M = J_{11})$	1.686, 18.36, 0.749

Table 2: Parameters of joint torque controller.

Left side driveshaft torque reference $T_{Lds-ref}$	-450 Nm
Right side driveshaft torque reference $T_{Rds-ref}$	450 Nm
Rate limiter for $T_{jds-ref}$	± 2000 Nm/s
Cutoff frequency of Q_{FF}	10 Hz

While this JTC–s0 is very simple to implement and theoretically eliminates inertia torque coupling and offsets, vibration caused by elastic and damping elements is expected to remain. Yet again, since a controller with no dynamics (i.e. $s = 0$) is convenient for the practical implementation, JTC–s0 will be compared as well. The left and right wheels are driven with independently different reference torque values for three seconds. In each case, the vehicle accelerates from a stand still condition. The reference driveshaft torque $T_{jds-ref}$ changes in a "step manner" with a rate limiter of 2000 N/s. Tab. 1 and Tab. 2 show the specification of the simulated vehicle and parameters of the JTC.

4.2 Simulation results Fig. 9 shows the simulation results of the JTC for TDA-TVD. In the figures, subscription "ref", "wo", "E+FF(s=0)", and "E+FF" suggest the reference value of the driveshaft torque (blue dashed line), measured value with the base control (red line), with JTC–s0 (green line), and with full JTC (black line), respectively. Fig. 9(a) and Fig. 9(b) show the driveshaft torque T_{Rds} and T_{Lds}.

Obviously, the base control (without the JTC, red line) has the largest vibration and overshoot of all cases. In addition, since the base control does not consider the motor inertia torque at all, a certain offset error remains. The magnitude and degree of the offset error depend on the torque difference between the left and right wheels. The wheel which has the largest torque input always has a smaller driveshaft torque value compared to the reference value, and vice versa.In the case of the JTC–s0, it reduces the offset error regardless of the torque difference. However, the vibration still remains, naturally. On the other hand, the full JTC reduces the joint torque vibration significantly. Furthermore, during the transition, driveshaft torques follow the reference values almost without delay.

5. Experimental validations of the joint torque controller for TDA-TVD

Experimental validation of the JTC for TDA-TVD is conducted using a real vehicle with the TDA-TVD unit. The experimental vehicle is shown in Fig. 10. The experimental vehicle is equipped with a device that can measure driveshaft torques T_{jds} on both sides.

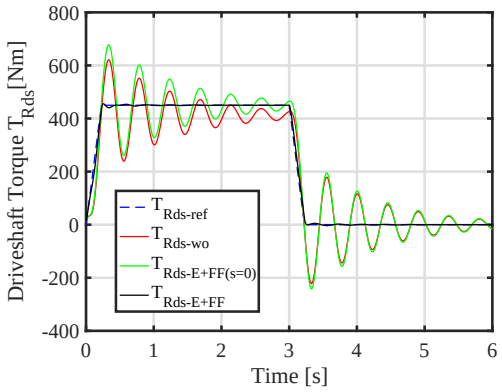

(a) Driveshaft torque T_{Rds}.

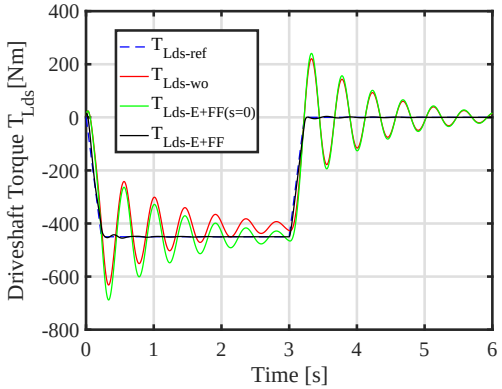

(b) Driveshaft torque T_{Lds}.

Figure 9: Simulation results.

Figure 10: Experimental vehicle equipped with TDA-TVD.

5.1 Test of the decoupling compensator To confirm the effect of the designed decoupling compensator, the experimental vehicle is lifted and we attempt to rotate the left side wheel by giving some non-zero driveshaft torque reference $T_{Lds-ref}$ only to the left side wheel using the decoupling compensator.

Fig. 11 shows the results of the test. Without the decoupling compensator (Fig. 11(a)), both wheels started to rotate due to the motor side inertia coupling. On the other hand, with the decoupling compensator (both for the full JTC and JTC–s0), the right side driveshaft torque T_{Rds} maintains around 0 Nm for around 3s, and the right side wheel was successfully kept to zero rotation speed until 4s. The viscosity of TDA-TVD (inside the planetary gear unit) is another coupling element and it leads to the rotation of the other side of the wheel. This viscosity is currently not modeled and its identification and compensation will be future work.

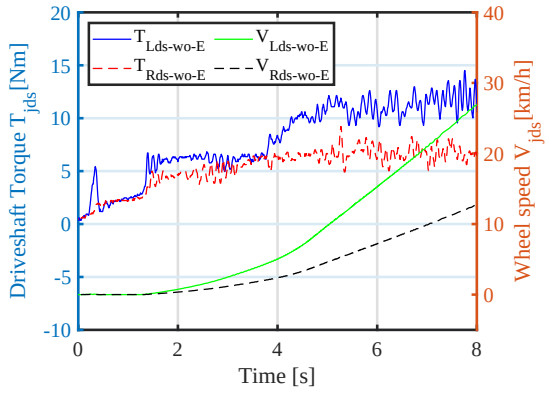

(a) Without decoupling compensator.

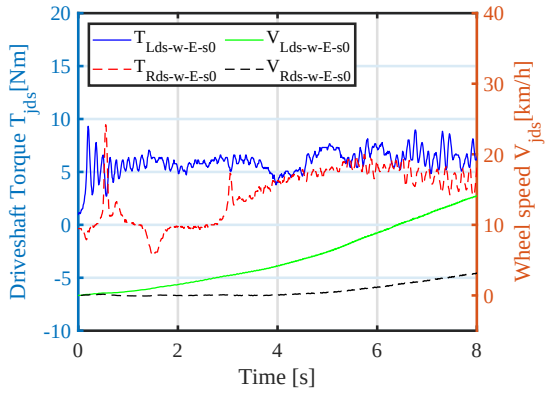

(b) With decoupling compensator ($s = 0$).

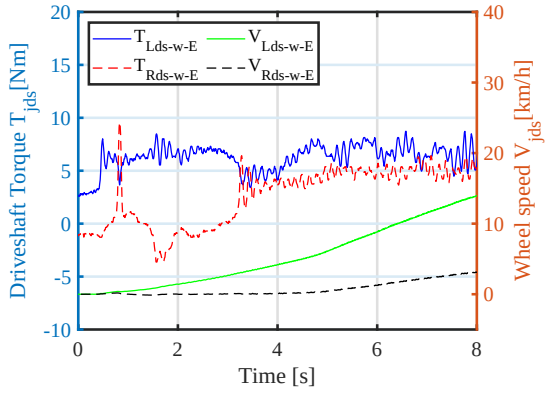

(c) With decoupling compensator.

Figure 11: Test results of the decoupling compensator.

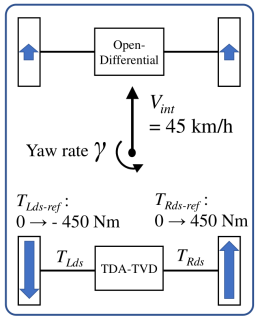

Figure 12: Illustration of the experiment.

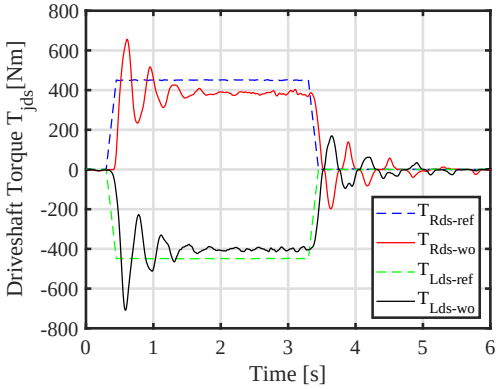

(a) Driveshaft torque T_{jds}.

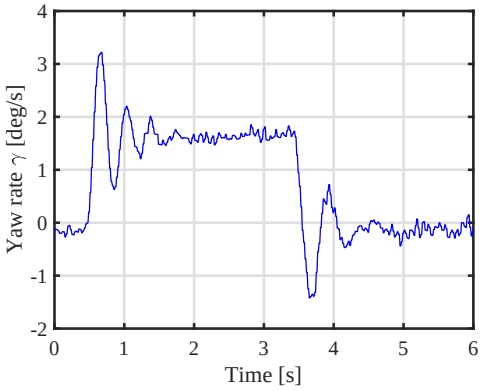

(b) Yaw rate γ.

Figure 13: Experimental results without JTC.

Table 3: Evaluation of joint torque controller.

	Without JTC	JTC–s0	JTC
Offset error e_{TRds} [%]	-14.1	-7.4	-5.4
Overshoot OS_{TRds} [%]	69.8	70.2	18.2
Settling time t_{s-TRds} [s]	1.19	1.19	0.80
Overshoot OS_{γ} [%]	100.0	115.0	23.4
Settling time $t_{s-\gamma}$ [s]	1.21	1.21	1.23

Overall, the decoupling compensator effectively reduces the coupling between the left and right wheels, but further modeling of the viscosity coupling will improve the decoupling performance.

5.2 Experimental conditions Fig. 12 illustrates the experimental verification. The experimental vehicle goes on a straight path at a speed of 45 km/h driven by the front wheels. Then, the rear wheels are driven with a torque difference of 900 Nm for 3 seconds, which is the same condition with the simulation shown earlier. While the torque vectoring system is working, the steering angle is maintained at 0 degree by the driver.

The JTC is implemented with the vehicle parameters of the experimental vehicle. The equivalent stiffness and damping factor of the driveshaft (K_s and D_s) of the experimental vehicle were estimated by measuring the driveshaft torque of the step response. Correspondingly with the simulation, both sides of the driveshaft torque T_{jds} are measured and their responses are evaluated with three situations: without the JTC, with the JTC–s0, and with the full JTC. Yaw rate γ is also measured and evaluated.

5.3 Experimental results Figs. 13-15 show the experimental results of the JTC for TDA-TVD. There are large vibrations of the measured driveshaft torques T_{jds} and yaw

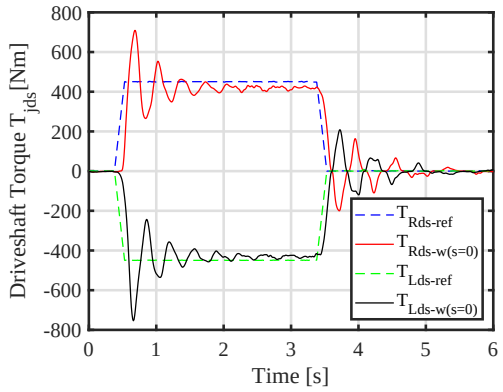

(a) Driveshaft torque T_{jds}.

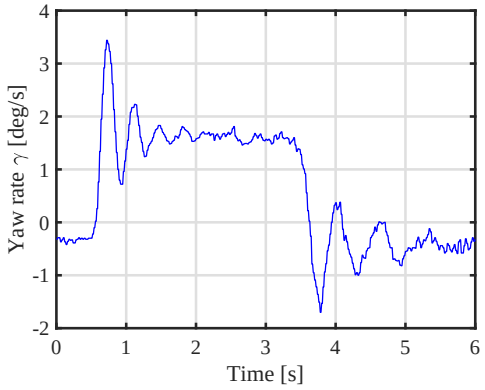

(b) Yaw rate γ.

Figure 14: Experimental results with JTC–s0.

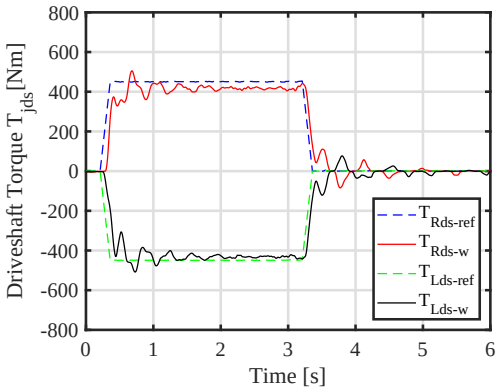

(a) Driveshaft torque T_{jds}.

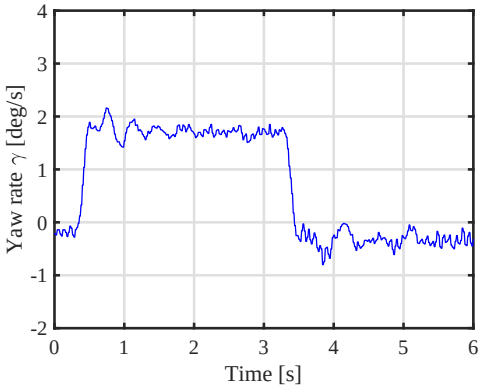

(b) Yaw rate γ.

Figure 15: Experimental results with JTC.

rate γ with the base control (without the JTC, Fig. 13), in addition to the non-negligible offset error. With the JTC–s0, the offset error is cut by about half compared to the base control. However, as expected, the vibrations of the measured driveshaft torques T_{jds} and yaw rate γ remain. On the other hand, both vibrations are considerably reduced with the JTC. Overshoots of driveshaft torques T_{Rds} and yaw rate γ become about one third and one fourth, respectively. Furthermore, the rise of the driveshaft torques T_{jds} becomes rather slightly sharper, without compromising the response.

Tab. 3 quantitatively shows the performance of each of the controllers. On the table, e_{TRds} is the offset error of the right side driveshaft torque T_{Rds} between the settling value and the reference value. Overshoot OS_{TRds} is the difference between the value of the first peak and the settling value of the right side driveshaft torque T_{Rds}. Settling time t_{s-TRds} is the duration between the moment T_{Rds} settles within ±5% of the settling value. Overshoot OS_{γ} and settling time $t_{s-\gamma}$ are defined in the same way.

Overall experimental results confirm the validity of the derived dynamic model of TDA-TVD, the effectiveness of the decoupling compensator and the feedforward controller. However, offset errors still remain likely due to the unmodeled/neglected elements such as the coupling cause by a certain viscosity between the left and right wheels (i.e. planetary gears), and the inertia of gears. Better tracking and control of the driveshaft torque T_{jds} could be achieved by more a detailed system identification including the aforementioned elements and its investigation will be future work. Furthermore, co-use of the feedback controller and various conventionally proposed vibration suppression algorithms could improve the performance as well and will also be investigated in the future.

6. Conclusion

This study proposed a dynamic model and a decoupling compensator of a two-input-two-output torque vectoring differential with torque difference amplification (TDA-TVD) for electrified vehicles in order to achieve both independent drive of the left and right wheels and improved controllability. The decoupled system of TDA-TVD can be treated as an Individual-wheel-drive (IWD) system and any conventional vehicle dynamics and motor drive controllers for IWD system can be applied. As a benchmark, a feedforward-based vibration suppression controller was applied and tested. The results of experimental evaluations using a real vehicle with a TDA-TVD unit showed that both the driveshaft torque and yaw rate vibrations were reduced to about 25% compared to the baseline without any control while the torque vectoring is in function. The process of modeling of any two-input-two-out-put motor drive systems and designing of its controllers will be significantly more efficient with the proposed approach. An improved and more detailed system identification of TDA-TVD such as the viscosity coupling, implementation of an additional feedback controller, and further improvement of the vibration reduction will be future work.

References

(1) Y. Shibahata, K. Shimada, and T. Tomari, "Improvement of vehicle maneuverability by direct yaw moment control," Veh. Syst. Dyn., vol. 22, no. 5-6, pp. 465-481, 1993.

(2) K. Sawase, Y. Ushiroda, and T. Miura, "Left-right torque vectoring technology as the core of super all wheel control (S-AWC)," Mitsubishi Motors Tech. Rev., vol. 18, pp. 16-23, 2006.

(3) L. Zhang, H. Ding, Y. Huang, H. Chen, K. Guo and Q. Li, "An Analytical Approach to Improve Vehicle Maneuverability via Torque Vectoring Control: Theoretical Study and Experimental Validation," IEEE Trans. on Vehicular Technology, vol. 68, no. 5, pp. 4514-4526, May 2019.

(4) Y. Hori, "Future vehicle driven by electricity and control research on four-wheel-motored 'UOT electric march II'," IEEE Trans. on Industrial Electronics, 51, 5, pp. 954-962, 2004.

(5) Y. Chen, S. Chen, Y. Zhao, Z. Gao and C. Li, "Optimized Handling Stability Control Strategy for a Four In-Wheel Motor Independent-Drive Electric Vehicle," in IEEE Access, vol. 7, pp. 17017-17032, 2019.

(6) M. Chae, Y. Hyun, K. Yi and K. Nam, "Dynamic Handling Characteristics Control of an in-Wheel-Motor Driven Electric Vehicle Based on Multiple Sliding Mode Control Approach," in IEEE Access, vol. 7, pp. 132448-132458, 2019.

(7) Sawase. K, Chiba M, "Study of Lateral Torque-vectoring Differential Suitable for Electric Powered Vehicles," Transactions of Society of Automotive Engineers of Japan, Vol.45-5, p.823-828, 2014 (In Japanese).

(8) Sawase. K, et.al., "Classification and Analysis of Torque-vectoring Differentials with Torque Difference Amplification Mechanism," Transactions of Society of Automotive Engineers of Japan, Vol.48, No.2, p.317-322, 2017 (In Japanese).

(9) H. Kawamura, K. Ito, T. Karikomi, and T. Kume, "Highly-Responsive Acceleration Control for the Nissan LEAF Electric Vehicle," SAE Technical Paper 2011-01-0397, 2011.

(10) A. Scamarcio, M. Metzler, P. Gruber, S. De Pinto and A. Sorniotti, "Comparison of Anti-Jerk Controllers for Electric Vehicles With On-Board Motors," IEEE Transactions on Vehicular Technology, vol. 69, no. 10, pp. 10681-10699, Oct. 2020.

(11) H. Sumiya and H. Fujimoto, "Driving Force Control Method Using Suppression Control of Driving-shaft Vibration for Electric Vehicle with On-board Motor," in Proc. IEEJ Industry Applications Society Conf, no. 106, 2012, pp. 115–120 (in Japanese).

(12) S. Wakui, T. Emmei, H. Fujimoto, Y. Hori, "Gear Collision Reduction of Geared In-wheel-motor by Effective Use of Load-side Encoder," The 45th Annual Conference of the IEEE Industrial Electronics Society, Lisbon, Portugal, pp.3469-3474, 2019.

(13) W. Ohnishi, et. al, "Decoupling Control Method for High-Precision Stages using Multiple Actuators considering the Misalignment among the Actuation Point, Center of Gravity, and Center of Rotation", IEEJ Journal of Industry Applications, Vol.5, No.2, pp.141-147, 2016.

Hiroyuki Fuse (Student Member) was born in 1994. He received the B.Eng. degree in Electrical and Electronic Engineering from the Tokyo Institute of Technology in 2017, and the M.S. degree of Advanced Energy from the University of Tokyo in 2019. He is currently pursuing a Ph.D. degree in the Department of Advanced Energy, the University of Tokyo, Japan. He received the JSAE Graduate School Research Award in 2019, IEEJ Excellent Presentation Award in 2019, and the Dean's Award for Outstanding Achievement from the Graduate School of Frontier Sciences and Faculty of Engineering, the University of Tokyo in 2019. His current research interests include vehicle dynamics, drivability improvements and motion control of electric vehicles. He is a student member of IEEE and SAE of Japan, respectively.

Hiroshi Fujimoto (Senior Member) received the Ph.D. degree in the Department of Electrical Engineering from the University of Tokyo in 2001. In 2001, he joined the Department of Electrical Engineering, Nagaoka University of Technology as a research associate. From 2002 to 2003, he was a visiting scholar in the School of Mechanical Engineering, Purdue University, U.S.A. In 2004, he joined the Department of Electrical and Computer Engineering, Yokohama National University, Yokohama, Japan, as a lecturer and he became an associate professor in 2005. He is currently an associate professor of the University of Tokyo since 2010. He received the Best Paper Awards from the IEEE Transactions on Industrial Electronics in 2001 and 2013, Isao Takahashi Power Electronics Award in 2010, Best Author Prize of SICE in 2010, the Nagamori Grand Award in 2016, and First Prize Paper Award IEEE Transactions on Power Electronics in 2016. His interests are in control engineering, motion control, nano-scale servo systems, electric vehicle, motor drive, visual servoning, and wireless motors. He is a senior member of IEE of Japan. He is also a member of the Society of Instrument and Control Engineers, the Robotics Society of Japan, and the Society of Automotive Engineers of Japan. He is an associate editor of IEEE/ASME Transactions on Mechatronics from 2010 to 2014, IEEE Industrial Electronics Magazine from 2006, IEE of Japan Transactions on Industrial Application from 2013, and Transactions on SICE from 2013 to 2016. He is a chairperson of JSAE vehicle electrification committee from 2014 and a past chairperson of IEEE/IES Technical Committee on Motion Control from 2012 to 2013.

Kaoru Sawase (Non-member) was born in Japan, May 1963. He received the B.E. and the M.E. degrees in precision engineering in 1986 and 1988, and Ph.D. degree in mechanical system design engineering in 2009 from Tohoku University, respectively. From April 1988 to December 2011, he worked for Mitsubishi Motors. From April 2012 to March 2017, he was a professor of National Institute of Technology, Ichinoseki College. He is currently a Chief Technology Engineer in Mitsubishi Motors. He received JSAE Award in 2008 and IMechE Part D: Journal of Automobile Engineering 2009 Best Paper Award Highly Commended in 2010. He is a JSAE Fellow Engineer since 2018.

Naoki Takahashi (Non-member) received the B.E. degree in mechanical engineering in 1998 from Tokyo University of Science. He is currently working for Mitsubishi Motors since 1998.

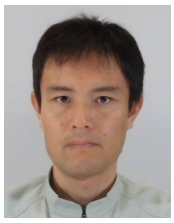

Ryota Takahashi (Non-member) received the B.E. degree in mechanical system engineering in 2007 from Yamagata University. He is currently working for Mitsubishi Motors since 2011.

Yutaro Okamura (Non-member) received the B.E. degree in functional machinery and mechanics course, faculty of textile science and technology in 2018 from Shinshu University. He is currently working for Mitsubishi Motors since 2018.

Ryosuke Koga (Non-member) received the B.E. degree in engineering system in 2008 from University of Tsukuba, and the M.E. in systems and information engineering from University of Tsukuba in 2010. He is currently working for Mitsubishi Motors since 2011.